A Derivative of Stick Filter for Pulmonary Fissure Detection in CT Images

Changyan Xiao[a], Marius Staring[b], Juan Wang[a], Denis P. Shamonin[b] and Berend C. Stoel[b]

[a]College of Electrical and Information Engineering, Hunan University, Changsha, P. R. China;
[b]Division of Image Processing, Department of Radiology, Leiden University Medical Center, Leiden, The Netherlands

ABSTRACT

Pulmonary fissures are important landmarks for automated recognition of lung anatomy and need to be detected as a pre-processing step. We propose a derivative of stick (DoS) filter for pulmonary fissures detection in thoracic CT scans by considering their thin curvilinear shape across multiple transverse planes. Based on a stick decomposition of a local rectangular neighborhood, a nonlinear derivative operator perpendicular to each stick is defined. Then, combining with a standard deviation of the intensity along the stick, the composed likelihood function will take a strong response to fissure-like bright lines, and tends to suppress undesired structures including large vessels, step edges and blobs. Applying the 2D filter sequentially to the sagittal, coronal and axial slices, an approximate 3D co-planar constraint is implicitly exerted through the cascaded pipeline, which helps to further eliminate non-fissure tissues. To generate a clear fissure segmentation, we adopt a connected component based post-processing scheme, combined with a branch-point finding algorithm to disconnect the residual adjacent clutters from the fissures. The performance of our filter has been verified in experiments with a 23 patients dataset, where pathologies to different extents are included. The DoS filter compared favorably with prior algorithms.

Keywords: Pulmonary fissure, image enhancement, segmentation, stick derivative.

1. INTRODUCTION

Pulmonary fissures are double layers of invaginations of visceral pleura that locate inside and anatomically separate the lungs.[1] There are two types of pulmonary fissures: normal and accessory fissures. Normal or lobar fissures are the physical boundaries of pulmonary lobes. Generally, they divide the human lungs into five distinct lobes (i.e. left upper, left lower, right upper, right middle and right lower lobes). Accessory fissures often occur between bronchopulmonary segments but may also enter subsegmental or interbronchial planes. Pulmonary fissures are important landmarks for delineation of pulmonary anatomy, and have significant value in localization of lesions and assessment of disease processes.[2] However, automated or computer-aided segmentation of pulmonary fissures in CT images is not an easy task. The main challenges come from their very thin, weak and varying structures, along with high-level imaging noise and interferences from adjacent tissues like vessels.

Many methods have been presented to realize automatic or semi-automatic segmentation of pulmonary fissures. To overcome the difficulty of insufficient information, various kinds of prior knowledge have been merged into a framework of fissure detection. These include the sparse distribution of vessels and bronchi around the fissures,[3,4] single- or multi-atlas of pulmonary anatomy,[5,6] and the curved surface shape of fissure appearance.[7–10] Among them, the first two are indirect constraints, while the third one comes directly from the object and is believed more reliable for accurate localization.[11]

Following the prior shape merging strategy, we will present a nonlinear filter for fissure detection with emphasis on improving the estimation of fissure direction and suppression of adjacent interference. Motivated by a line detection model in speckle images,[12] our basic idea is to iteratively probe the presence of bright lines across multiple transverse planes. Considering the locally linear shape of fissures inside each slice plane, a 2D prober is

Further author information:
Changyan Xiao (E-mail: C.Xiao@hnu.edu.cn), Marius Staring (E-mail: M.Staring@lumc.nl).

Table 1. Decomposition of a 9×9 rectangle neighborhood with stick kernels.

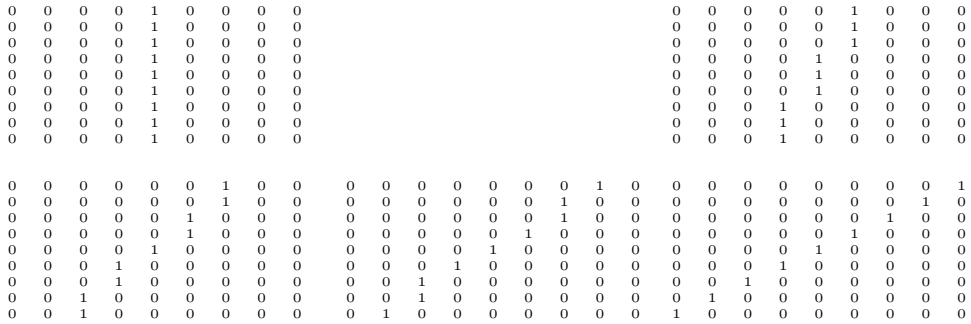

defined by decomposing the rectangle neighborhood into different line-segments or sticks with varying orientation. Then, the nonlinear derivatives perpendicular to each stick along with its intensity variance are combined to generate a new fissure likelihood measure. With a cascading pipeline implementation, our filter is able to enhance fissure-like thin plane structures, while suppressing undesired pulmonary tissues like large vessels and bronchi. In this paper, our main purpose is to extract pure fissure objects rather than generate a full lobe segmentation. This means that neither extrapolation is adopted to extend the extracted fissure plane to lung boundaries, nor interpolation is used to fill its inner holes.

2. METHODS

If we cut the volume lung CT image using multiple planes with different orientations, the fissures will typically appear as bright thin curved lines through all the cross-sections. This observation is considered an important feature to discriminate the fissures from other pulmonary structures. For example, the small vessel might happen to be a thin line inside a transverse plane, but it does not simultaneously takes a similar shape in the orthogonal cross-section.

Based on this, we will propose a method for fissure enhancement in volume CT images using an iteration pipeline, where the 2D line filters across three orthogonal transverse planes are cascaded together. In this section, our main work includes the 2D line filter design and a post-processing algorithm for clutters removal.

2.1 Stick decomposition of neighborhood

A problem with pulmonary fissures detection in CT images is that they often appear to be single-pixel wide and even broken for several pixels. The traditional isotropic smoothing schemes are inappropriate here, because they might sweep out the weak fissures together with the noise. This can also explain the weakness of some Hessian or structure tensor based fissure filters,[13] which depend on a low-level Gaussian smoothing to calculate the derivatives. Instead, we adopt a realistic way to test the intensity distribution by probing it with straight line segments called sticks in varying orientations. The stick model decomposes a rectangle neighborhood into line segments with fixed length.[12] Typically, a $L \times L$ neighborhood can be decomposed into $2(L-1)$ sticks. See Table 1 for examples with $L = 9$; The other sticks can be easily obtained by rotating the listed ones.

To some extent, the stick-based smoothing can be considered an extreme case of oriented anisotropic Gaussian filters,[14] where the long axis scale is much larger than the one along the short axis. Additionally, a simple rectangular window average is used to replace the original Gaussian weighting. This minimizes the influence of relative position in the kernel, and will help to preserve axial continuity even if the central point gets a lower intensity.

2.2 Definition of a nonlinear derivative

On basis of the stick decomposition, a new filter can be developed by introducing a triple of parallel sticks. As shown in Fig. 1, using μ_M, μ_L and μ_R to indicate the mean intensity respectively along the middle and the two side sticks, a nonlinear operator perpendicular to the sticks is defined as

$$\lambda_{\perp}^{s} = \min(\mu_M - \mu_L, \mu_M - \mu_R). \tag{1}$$

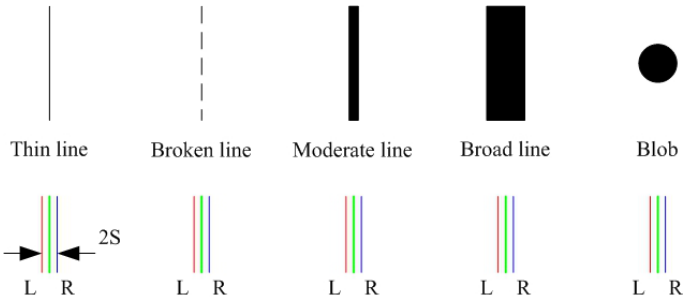

Figure 1. Analyzing the property of the stick derivative $\lambda^s_{\perp}$ on different pulmonary structures. Here, the gray-levels are inversely displayed.

With a spacing parameter S involved in the template, the operator is less sensitive to partial volume effects, and allow the fissures with varying width or blurring boundaries to be equally well detected. Additionally, due to the sparseness or lack of vessels and bronchi, the adjacent background on both sides of the fissures also takes a low-intensity narrow ribbon shape. Therefore, the usage of triple sticks to simultaneously probe the linear fissure object and its close neighborhood is more like the inference of human observers. Here, the $\min(\cdot)$ in Eq. (1) is adopted particularly for suppression of step edges, which often correspond to the large vessel and lung boundaries. Note a similar scheme was presented by Hunter et al.[15] as the tram-line filter in retinal vessel segmentation. Our method differs from the tram-line filter in that the triple stick derivative only contributes to a single directional contrast in our line likelihood definition, and an order statistic filtering for the minimax combination was used in their work.[15] To analyze the property of our nonlinear derivative measure, some idealized shapes representing different pulmonary structures are illustrated in Fig. 1. Here, the thin, broken and moderate lines corresponding to various fissure appearances will give a high value of $\lambda^s_{\perp}$. The broad line, which indicates the large vessels or step-edges, will be neglected with a null response. However, for the blob-shaped interference, the $\lambda^s_{\perp}$ will not give the full response, but also not a zero response.

As a remedy for this false response to blobs, we introduce a second measure $\lambda^s_{\shortparallel}$ equal to the standard deviation of the pixel intensity along the middle stick. The utilization of intensity variance to detect linear edges was inspired by our previous work.[16] Like the popular lineness or vesselness filters,[17,18] $\lambda^s_{\perp}$ and $\lambda^s_{\shortparallel}$ are similar to the Hessian eigenvalues: they also reflect the local contrast in the two principal directions. Accordingly, a 2D fissure likelihood function can then be defined as

$$\ell^s = \lambda^s_{\perp} - \kappa \cdot \lambda^s_{\shortparallel}. \tag{2}$$

Here, κ is a positive coefficient to punish axial intensity inhomogeneity. Obviously, the blob structure shown in Fig. 1 will get a low response under Eq. (2) due to its large intensity variation along the middle stick.

2.3 Multi-direction integration and implementation

As depicted in Table 1, a rectangular neighborhood is decomposed into sticks with varying orientations. We choose the stick template with the maximum response of Eq. (2) as the optimal kernel. Thus, the multi-directional information can be integrated with

$$\ell^s_m(x_1, x_2) = \max\{\ell^s_i, 1 < i < 2(L-1)\}. \tag{3}$$

Here, ℓ^s_i indicates the linear likelihood estimation of the ith stick. To reduce the heavy burden in computation of $\lambda^s_{\perp}$, we adopt a simplified spatial shifting scheme to replace the original triple stick template. That means only the $\mu_M(x_1, x_2)$ need calculating in Eq. (1), while $\mu_L(x_1, x_2)$ and $\mu_R(x_1, x_2)$ are respectively assigned to $\mu_M(x_1 \pm S, x_2)$ or $\mu_M(x_1, x_2 \pm S)$ depending on the approximately east-west or north-south direction of the template.

To realize 3D fissure enhancement in the volume data, we apply the 2D filter of Eq. (3) iteratively to the three transverse imaging planes. Although there exist many solutions to combine the 2D filtering responses from different planes, a cascading pipeline is verified to be a good choice in our experiments. Note some fissure

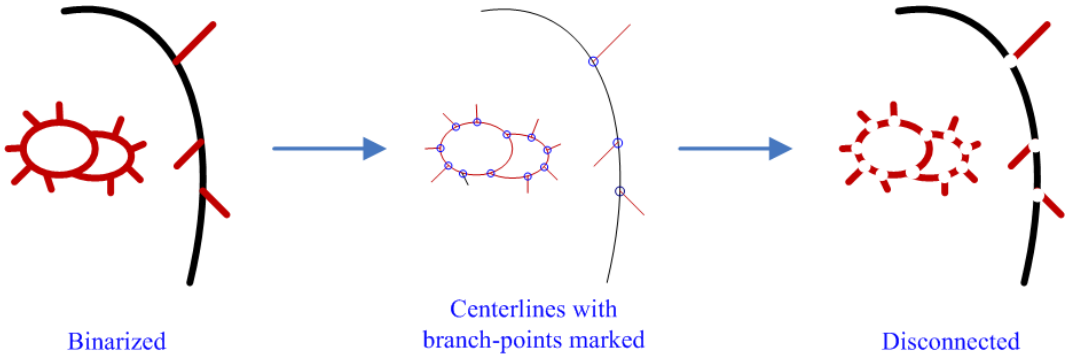

Figure 2. Disconnect clutters with a branch-point finding algorithm. Here, the black curves indicate the real fissures and the red ones being the clutters.

segments especially those belonging to the horizontal fissures often run along the axial plane, they are subject to being missed in thick-slice scans or frequently take a vague band appearance. In those cases, the fissure object tends to be misinterrupted by the line prober. Comparatively, across the sagittal plane, both oblique and horizontal lobar fissures are more likely to take a clear thin curvilinear shape. Therefore, our filtering adopts a fixed cascading order from the sagittal slices to the coronal and finally the axial slices. The specific sequence helps to minimize the influence of imaging orientation, since the axially ambiguous objects can be gradually sharpened and thinned with processing in sagittal and coronal directions. Although we use no strict 3D planar template for local fissure matching like previous authors[19] , the 2D linear shape constraints through multiple transverse planes can be considered a realistic simplification, and its obvious merit is a large decrease of computational burden.

2.4 Post-processing algorithms

To remove clutters especially those linking to the fissures, we introduce a post-processing scheme based on connected component analysis. The critical part is a 2D branch-point finding algorithm, which also works through the transverse planes. As shown in Fig. 2, our algorithm begins with a binarization of the previous filtered result using a global threshold. The threshold value should be chosen low enough to retain the majority of weak fissures. Generally, the width of the binarized objects will not exceed $2S$ due to the distinct combination of stick responses. Then, a morphological thinning algorithm[20] is adopted to extract the centerlines, and the branch-points can be marked with a simple neighborhood search according to an early definition.[21] After removing the branch-points and their circular neighborhoods with radius equal to S in the binarized slice, both fissures and clutters are broken into small segments through the specific cross-section. However, because the fissures are typically 3D surfaces, the removal of small 2D regions will seldom affect their connectivity in 3D space. But the clutters, which mainly come from the residual of pulmonary vessels and airway trees or pathological deformations like fibrosis, only dominate in a single direction and is prone to be split into small fragments after the sequential deletion of branch-points. Therefore, based on a 3D connected component analysis, a simple labeling and volume comparison can easily sift out the desired objects.

3. EXPERIMENTS AND EVALUATION

Presently, our algorithms were implemented in Matlab (MathWorks Inc.). The runtime of the DoS filter for a typical $256 \times 512 \times 512$ size 3D image is around 810s on our computer, configured with a 2.67 GHz CPU, 8 GB memory and a 64-bit Windows 7 operating system.

3.1 Data and reference standard

The proposed filter has been verified in experiments using chest CT scans of 23 Chronic Obstructive Pulmonary Disease (COPD) patients from a previous study.[22] The images were acquired with a Toshiba Aquilion 16 CT scanner using the parameters: 120 kVp; 140 mAs per rotation; rotation time 0.4 s; collimation: 16×0.5 mm; and pitch factor: 1.4375. Images were reconstructed with a FC02 kernel (FOV of 295 - 400 mm; slice thickness 0.5

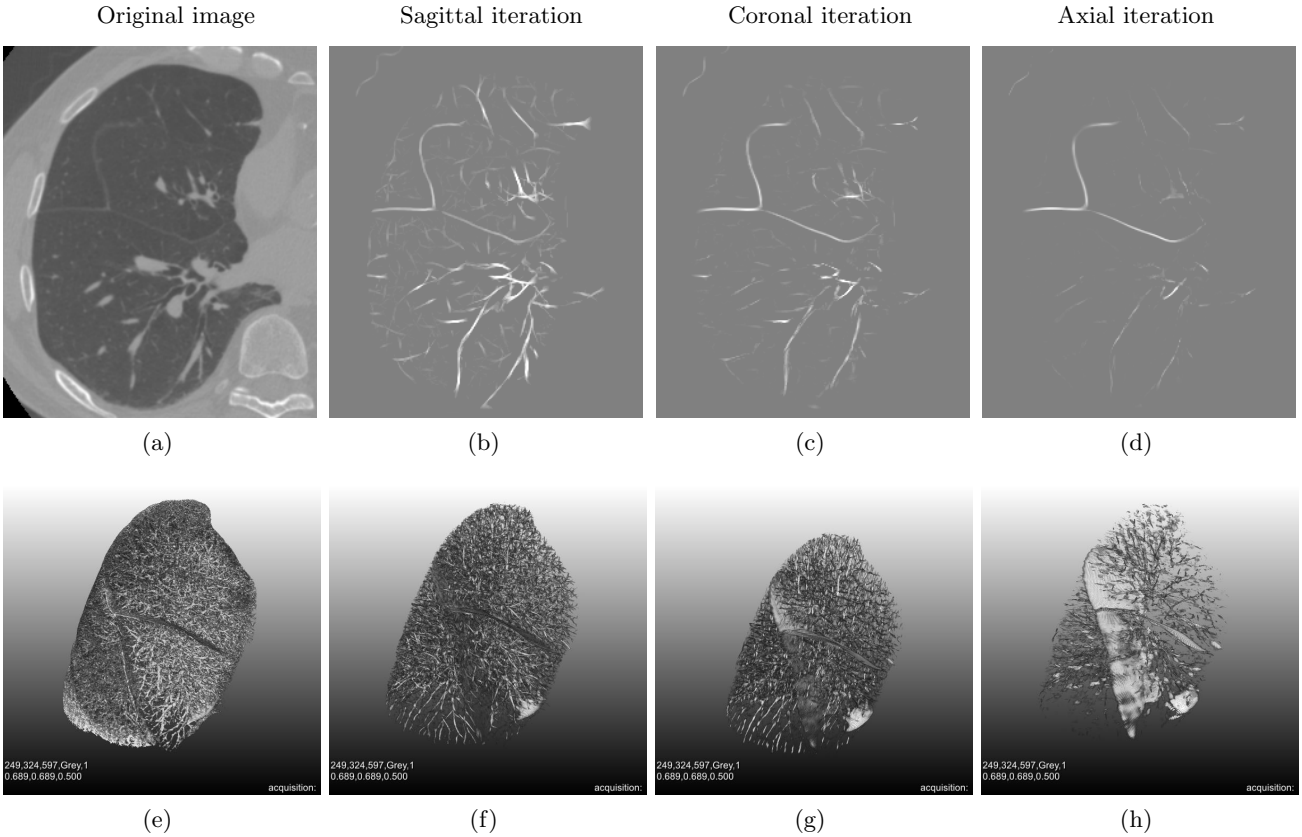

Figure 3. Applying the 2D DoS filter in a cascaded pipeline successively to the sagittal, coronal and axial planes with $L = 9$, $S = 3$, and $\kappa = 0.8$. The top row depicts one axial slice, and the bottom row is the 3D visualization using volume rendering. From left to right, the original image and the filtering results corresponding to iterations in three different cross-sections are respectively given.

mm; increment 0.5 mm). Scans were made during breath hold at full inspiration without contrast media. The patient group had moderate to severe COPD (GOLD stage II and III) without $\alpha 1$ antitrypsin deficiency; aged 49-78, and FEV1 between 36% and 87% predicted.

To evaluate the proposed method, the ground truth of lobar fissures was generated on basis of our previous lobe segmentations,[23] which were manually defined and have been approved by a pulmonologist. Since our purpose focuses on fissure detection rather than a complete lobe segmentation, the previously obtained lobe references, which involved interpolation and extrapolation, are not suitable here. Therefore, the ground truth was adapted as follows: We first automatically extracted the complete interlobar boundaries as a starting point using a morphological gradient calculation. Then, to purify the result, two trained operators further removed the non-fissure (invisible to observers) parts with an interactive editing tool developed in Mevislab,[24] a third observer subsequently verified the references and a radiologist was enquired to settle the disputes. Finally, a skeletonizing operation was applied to ensure a uniform single-pixel width through the fissure reference. In this paper, we only consider the lobar fissures (no accessory fissures). The major and minor fissures in the right lung are considered a single object, and then validated together without discrimination.

3.2 Experimental results

In the experiments, we used the parameters $L = 9$, $S = 3$, $\kappa = 0.8$ for the DoS filtering and a fixed global threshold of 0.5 for post-processing. The performance of our proposed DoS filter is demonstrated with the intermediate and final results on a COPD patient image in Fig. 3. Here, only the right lung is shown and a coarse lung segmentation was needed to mask out adjacent interferences like the ribs. As observed, the fissures are gradually enhanced through the iterations, though the highly curved parts appear to get a weaker response.

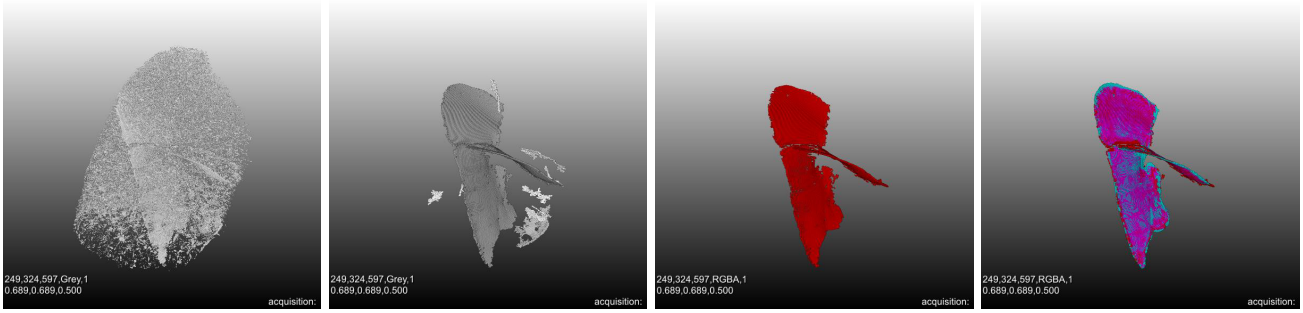

(a) (b) (c) (d)

Figure 4. Extracting pulmonary fissures with the post-processing algorithms, and an isosurface rendering technique is used for visualization. Here, (a) indicates the branch-point removed result after binarizing the fissure filter output with a global threshold 0.5, (b) corresponds to the 10 biggest objects, (c) represents the extracted fissure and its overlaying with the manually drawn reference is given in (d).

On the other hand, the densely distributed vasculature and airway trees, which is thought a main hurdle to fissure segmentation, have been largely suppressed. This can be seen across the 2D slices or through the 3D visualization.

Although the enhancement of fissures has largely benefited the final segmentation, the residual small vessels or bronchi walls especially those linking to the fissure objects still remain a problem. As described in Section 2.4, the post-processing algorithm mainly depends on a connected component analysis after removing the branch-points across each 2D slice of the binary volume. In the experiment, we adopted a fixed global threshold 0.5 for all 23 scans. To illustrate the effect of the post-processing algorithms, the 3D surface rendering of results corresponding to different stages are given in Fig. 4. Here, Fig. 4a indicates the binarization of Fig. 3h along with removal of branch-points. Due to a very low threshold being used, a large number of clutter fragments still appear. Then, using a connected component analysis, the unbroken fissure objects were sifted out. We kept the 10 biggest objects as labeled in Fig. 4b, where the desired lobar fissures usually have a lower label value according to their volume sorting. Theoretically, the right major and minor fissures should be respectively the first and second biggest objects, with the left major fissure being the biggest object among their corresponding labeled results. In a few cases, to realize a perfect segmentation, manual intervention is needed to select the real fissures among the 10 objects mainly related to pathological deformation or inherent discontinuity. But it is possible to develop a fully automatic method when more global prior constraints and anatomical knowledge are merged.[23] As shown in Fig. 4c and d, the extracted fissures are highly consistent with the manual reference.

3.3 Evaluation

To give a quantitative evaluation of our filtering performance, the Precision-Recall (PR) curves of the 23 filtered results are calculated with the manually extracted fissures as a ground truth. The left and right lungs are handled separately. Like our previous work,[18] the PR curves are calculated by binarizing the filtered result with varying global thresholds. Since the fissure width might change with location, we skeletonized the binarized result into single-pixel width before comparing. For the DoS filtering evaluation, we defined the Volume of Interest (VOI) as a narrowed region with 40 mm width around the manual reference, since the interferences located much far away have little influence to real segmentation. But for the post-processing segmentation validation, we adopted the full lung regions.

The pixels inside the *binary result* are classified as true positive (TP_1) or false positive (FP) depending on the overlap with the manual reference. We used a 3mm tolerance for the "overlapping" determination, i.e. those with a minimum distance less than 3mm from the reference are considered TP_1 and the rest being FP. Accordingly, the *reference* pixels are divided into TP_2 and false negative (FN) using the same overlapping criterion, where FN corresponds to those located more than 3mm from the binary result. Note the two true positive measures TP_1 and TP_2 are not always equal. To avoid the influence of unbalanced number of pixels, we use the normalized ratios $TP_1/(TP_1+FP)$, $FP/(TP_1+FP)$ and $FN/(TP_2+FN)$ instead for precision-recall calculation. As shown

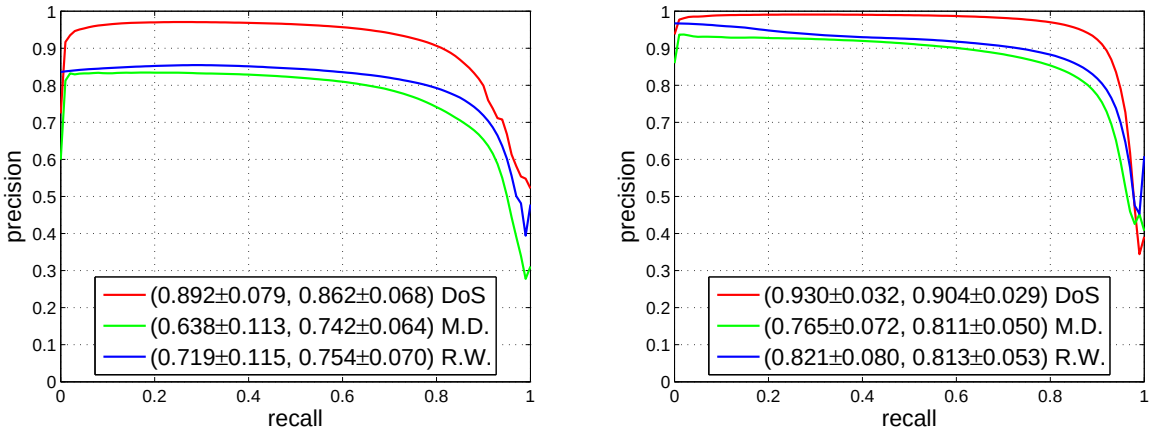

(a) Left lungs (b) Right lungs

Figure 5. Quantitative evaluation of fissure filtering using the Precision-Recall curves. Here, the proposed DoS filter is compared with the methods of M. Descoteaux (M.D.)[25] and R. Wiemker (R.W.).[13] The AUCs and max F_1-measures along with their standard deviations are given sequentially in the brackets of the legends.

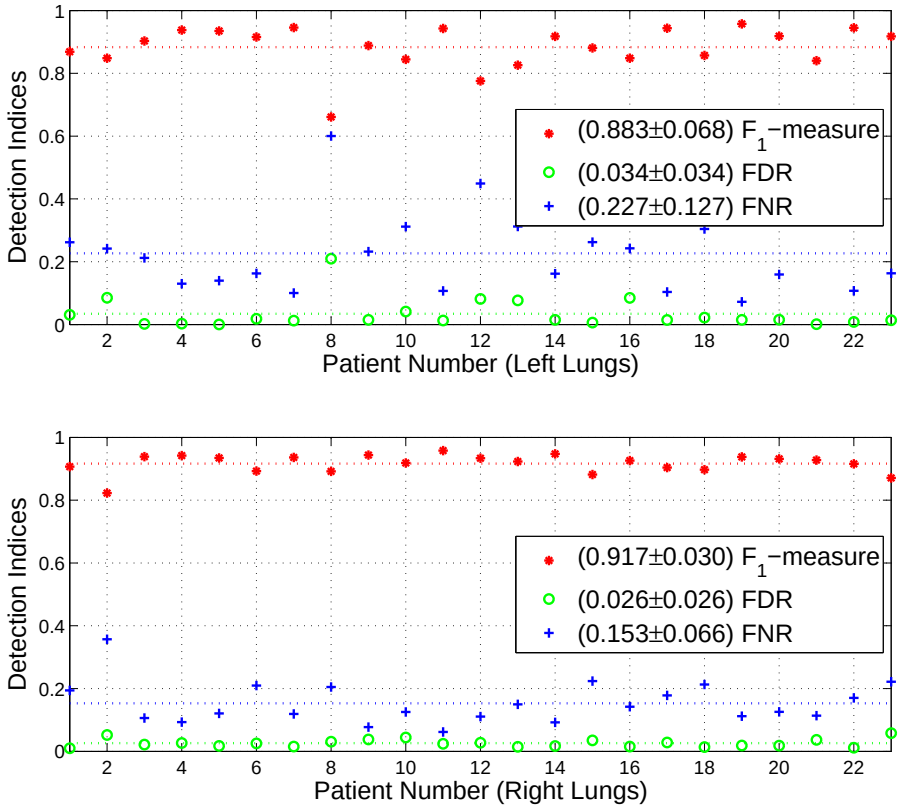

Figure 6. Evaluation of post-processed binary results using the F_1-measure, False Discovery Rate (FDR) and False Negative Rate (FNR) indices. The first and second rows correspond to the left and right lungs of the 23 COPD patient scans, respectively. Here, the means of the indices are drawn with dotted lines for references, and their digital values are given in the legends along with the standard deviations.

in Fig. 5, the PR curves corresponding to the left and right lungs of the DoS filtered results are respectively illustrated, where the area under the PR curve (AUC) and the maximum F_1-measure indices are given in the

legends. As a comparison, the results from two traditional fissure enhancement filters[13,25] are depicted together. Notice the F_1-measure is also known as the Dice similarity coefficient (DSC) in the literature.

The post-processed algorithms are validated by comparing their semi-automatic binary segmentations with the manually defined reference. Like the filtering evaluation, the agreement rate is measured with the F_1-measure and a 3mm distance threshold for overlapping determination is also used. To quantify the over- and under-segmentation errors, we introduce respectively the False Discovery Rate ($FDR = FP/(TP_1 + FP)$) and the False Negative Rate ($FNR = FN/(TP_2 + FN)$). As seen in Fig. 6, the performance on the right lungs is generally better than on the left lungs, indicated by higher F_1-measure and lower FDR and FNR indices. The main reason is that the left fissures more frequently take abnormal appearance along with disturbing background around the lung boundaries in our data set. Our computerized algorithm appears inferior to human observers to handle these complicated situations. On average, the FNRs are much higher than the FDRs, which reflects that "under-segmentation" is the main error source.

4. DISCUSSION AND CONCLUSION

We proposed a filter for pulmonary fissures detection in thoracic CT images. The prior surface shape of fissures in 3D space is simplified and transformed to an equivalent co-linear constraint across multiple transverse planes. A distinct feature is that we introduced a nonlinear combination of particularly designed anisotropic kernels, which makes it different from the conventional isotropic filters and can help to get more robust response even under serious noise and axial discontinuity. Moreover, with the definition of a new likelihood measure for thin linear shape, an obvious merit of our method is that the undesired interference structures are simultaneously suppressed along with the fissure enhancement. To obtain clear binary segmentation, our additional contribution is to develop a clutter disconnecting scheme based on 2D branch-points removal. It has been verified in experiments using clinical images that the proposed filter outperformed two conventional Gaussian derivative filters on both object detection and noise suppression.

With a purpose to suppress step-edges like lung and large vessel boundaries, the adoption of $\min(\cdot)$ operator in our filter unexpectedly brings some side effect. For example, as shown in Fig. 6, the fissures of the No. 8, 12 left lung and the No. 2 right lung images appear to be seriously undetected with very high FNRs. After investigating the original images, we found a large region of asymmetric roof or step-edge like fissures exist in these samples, which often generate a very low response under the minimum combination of stick responses. Another potential problem is with the thickened objects like double oblique fissures, which tend to be wrongly suppressed under the current derivative definition. These can be considered a principle limitation of the proposed filter and should be our research direction in the future. In spite of the shortcomings, the proposed method is able to provide a robust fissure segmentation in most cases using only direct intensity and shape information. This makes it of special value in applications like fissure integrity assessment.

Acknowledgment

This work was supported in part by National Science Foundation of China under Grant 61172160, the SRF for ROCS, SEM under Grant [2011] 1139, the NSF of Hunan Province under Grant 12JJ9019, and the FRF for the Central Universities of China.

REFERENCES

[1] Aziz, M., Ashizawa, K., Nagaoki, K., and Hayashi, K., "High resolution CT anatomy of the pulmonary fissures," *Journal Thoracic Imaging* **19**(3), 186–191 (2004).

[2] Cronina, P., Grossa, B. H., Kellya, A. M., Patela, S., Kazeroonia, E. A., and Carlosb, R. C., "Normal and accessory fissures of the lung: Evaluation with contiguous volumetric thin-section multidetector CT," *European Journal of Radiology* **75**(2), e1–e8 (2010).

[3] Kuhnigk, J., Hahn, H., Hindennach, M., Dicken, V., Krass, S., and Peitgen, H., "Lung lobe segmentation by anatomy-guided 3D watershed transform," *Proc. SPIE* **5032**, 1482–1490 (2003).

[4] Ukil, S. and Reinhardt, J., "Anatomy-guided lung lobe segmentation in x-ray CT images," *IEEE Transactions on Medical Imaging* **28**(2), 202–214 (2009).

[5] Zhang, L., Hoffman, E., and Reinhardt, J., "Atlas-driven lung lobe segmentation in volumetric x-ray CT images," *IEEE Transactions on Medical Imaging* **25**(1), 1–16 (2006).
[6] van Rikxoort, E., Prokop, M., de Hoop, B., Viergever, M., Pluim, J., and van Ginneken, B., "Automatic segmentation of pulmonary lobes robust against incomplete fissures," *IEEE Transactions on Medical Imaging* **29**(6), 1286–1296 (2010).
[7] Kubo, M., Niki, N., Nakagawa, S., Eguchi, K., Kaneko, M., Moriyama, N., Omatsu, H., Kakinuma, R., and Yamaguchi, N., "Extraction algorithm of pulmonary fissures from thin-section CT images based on linear feature detector method," *IEEE Transactions on Nuclear Science* **46**(6), 2128–2133 (1999).
[8] Wang, J., Betke, M., and Ko, J., "Pulmonary fissure segmentation on CT," *Medical Image Analysis* **10**(4), 530–547 (2006).
[9] van Rikxoort, E., van Ginneken, B., Klik, M., and Prokop, M., "Supervised enhancement filters: application to fissure detection in chest CT scans," *IEEE Transactions on Medical Imaging* **27**(1), 1–10 (2008).
[10] Pu, J., Leader, J., Zheng, B., Knollmann, F., Fuhrman, C., Sciurba, F., and Gur, D., "A computational geometry approach to automated pulmonary fissure segmentation in CT examinations," *IEEE Transactions on Medical Imaging* **28**(5), 710–719 (2009).
[11] Lassen, B., van Rikxoort, E., Schmidt, M., Kerkstra, S., van Ginneken, B., and Kuhnigk, J., "Automatic segmentation of the pulmonary lobes from chest CT scans based on fissures, vessels, and bronchi," *IEEE Transactions on Medical Imaging* (to appear) (2013).
[12] Czerwinski, R. and Jones, D., "Line and boundary detection in speckle images," *IEEE Transactions on Image Processing* **7**(12), 1700–1714 (1998).
[13] Wiemker, R., Blow, T., and Blaffert, T., "Unsupervised extraction of the pulmonary interlobar fissures from high resolution thoracic CT data," *ICS* **1281**, 1121–1126 (2005).
[14] Geusebroek, J.-M., Smeulders, A., and van de Weijer, J., "Fast anisotropic gauss filtering," *IEEE Transactions on Image Processing* **12**, 938–943 (2003).
[15] Hunter, A., Lowell, J., Ryder, R., Basu, A., and Steel, D., "Tram-line filtering for retinal vessel segmentation," in [*EMBEC 2005*], **11** (2005).
[16] Xiao, C., Zhang, S., and Chen, Y., "A diffusion stick method for speckle suppression in ultrasonic images," *Pattern Recognition Letters* **25**(16), 1867–1877 (2004).
[17] Frangi, A. F., Niessen, W. J., Vincken, K. L., and Viergever, M. A., "Multiscale vessel enhancement filtering," in [*MICCAI'98*], *Lecture Notes in Computer Science* **1496**, 130–137 (1998).
[18] Xiao, C., Staring, M., Shamonin, D. P., Reiber, J. H. C., Stolk, J., and Stoel, B. C., "A strain energy filter for 3D vessel enhancement with application to pulmonary CT images," *Medical Image Analysis* **15**, 112–124 (2011).
[19] Saita, S., Kubo, M., Kawata, Y., Niki, N., Ohmatsu, H., and Moriyama, N., "An algorithm for the extraction of pulmonary fissures from low-dose multislice CT image," *Systems and Computers in Japan* **37**(9), 63–67 (2006).
[20] Lam, L., Lee, S.-W., and Suen, C. Y., "Thinning methodologies-a comprehensive survey," *IEEE Transactions on Pattern Analysis and Machine Intelligence* **14**(9), 869–885 (1992).
[21] Arcelli, C. and di Baja, G., "Skeletons of planar patterns," *Machine Intelligence and Pattern Recognition* **19**, 99–143 (1996).
[22] Lapperre, T., Postma, D., Gosman, M., Snoeck-Stroband, J., ten Hacken, N., Hiemstra, P., Timens, W., Sterk, P., and Mauad, T., "Relation between duration of smoking cessation and bronchial inflammation in COPD," *Thorax* **61**(2), 115–121 (2006).
[23] Shamonin, D., Staring, M., Bakker, M., Xiao, C., Stolk, J., Reiber, J., and Stoel, B., "Automatic lung lobe segmentation of COPD patients using iterative B-spline fitting," in [*Medical Imaging 2012*], *SPIE Proceedings* **8314**, 83140W–83140W–7 (2012).
[24] Ritter, F., Boskamp, T., Homeyer, A., Laue, H., Schwier, M., Link, F., and Peitgen, H.-O., "Medical image analysis: A visual approach," *IEEE Pulse* **2**(6), 60–70 (2011).
[25] Descoteaux, M., Audette, M., Chinzei, K., and Siddiqi, K., "Bone enhancement filtering: Application to sinus bone segmentation and simulation of pituitary surgery," *Computer Aided Surgery* **11**(5), 247–255 (2006).